MRS Communications (2012), 2, 127–132
© Materials Research Society, 2012
doi:10.1557/mrc.2012.21

MRS Communications

Research Letters

Cu precipitation on dislocation and interface in quench-aged steel

Qingdong Liu* and **Shijin Zhao,** Key Laboratory of Microstructures and Institute of Materials, Shanghai University, Shanghai 200072, P.R. China
*Address all correspondence to Qingdong Liu at **qdliu@shu.edu.cn**

(Received 17 May 2012; accepted 24 August 2012)

Abstract

The Cu precipitation in a quench-aged high-strength low-alloy steel is studied at the atomic scale by atom probe tomography and high-resolution transmission electron microscopy. The results indicate that the Cu precipitates greatly correlate with carbides in the aspect of distributional character, i.e., the two phases are prone to coprecipitate on the dislocations and/or interfaces (low angle boundaries of the martensite laths). The crystallographic defects have a significant effect on the sizes, morphology and composition of Cu precipitates with Ni and Mn segregation shell.

Cu precipitation strengthening plays an important role in the fabrication of high-strength low-alloy (HSLA) steels[1–3]. The nature of Cu precipitation and the actual distributional morphology of the Cu precipitates have a significant effect on or directly determine the strength and toughness of HSLA steels.[4–6] Cu precipitation can occur during continuous cooling of austenite by interphase precipitation and occur during isothermal ageing of martensite by dislocation-interacted precipitation.[7] In the former condition, the Cu precipitation greatly correlates with the kinetics of austenite decomposition.[8,9] In the latter condition, the Cu precipitation usually depends on the extent of thermal ageing.[10–13] The martensite lath boundaries and the dislocations favor the nucleation of Cu precipitates as well as the segregation of solute atoms and the precipitation of carbides. The reactions often overlap and occur on the fine scale.[14]

The structural, compositional and morphological evolutions of Cu precipitates in Cu precipitation reaction are of fundamental scientific interest. High-resolution transmission electron microscopy (HRTEM) investigations reveal that the structures of Cu precipitates follow a complicated BCC → 9R → 3R → FCC sequence during the precipitation reaction.[15–22] Atom probe tomography (APT) studies suggest that at the initial nucleation stage the developing BCC Cu precipitates contain an equal amount of Fe with Cu as well as a small amount of Ni and Mn. The Ni and Mn are prone to segregate to the precipitate/matrix heterophase interface at the later growth and coarsening stages of Cu precipitation.[23–31] At the same time, the structural and compositional evolutions of Cu precipitates are greatly size-dependent and are in association with the morphological evolutions from spherical to ellipsoidal and then rod-like shape.

Solute atom segregation to and Cu precipitation on dislocations and interfaces are the most difficult microstructural features to quantify.[32–36]. In this paper, we characterize the Cu precipitation on the crystallographic defects of dislocations and martensite lath boundaries in a quench-aged Cu-bearing HSLA steel using HRTEM and APT. The experimental steel is received in as-rolled plate with 32 mm in thickness from the Institute of Research of Iron and Steel (IRIS), Shagang Group, China. The steel, with a composition of 0.04 C, 0.24 Si, 0.84 Mn, 1.15 Cu, 1.94 Ni, 0.51 Mo, 0.50 Cr, 0.043 Nb, 0.009 Ti, 0.03 Al, 0.004 N, 0.007 P and 0.004 S (wt.%), is fully austenitized and solutionized at 900 °C for 30 min followed by quenching in water at 25 °C, and then isothermally aged at 500 °C for 4 h. The HRTEM observations are conducted in a JEOL 2010 F (Tokyo, Japan) at 200 kV. The thin foils for TEM are prepared by mechanically grinding sample slices to 80-μm thick and twin-jet electropolishing in a mixture of 90% alcohol and 10% perchloric acid at −30 °C under 50 V. The APT experiment, using an advanced Imago (now Cameca Instruments) local electrode atom probe (LEAP, 3000X HR, CAMECA, Gennevilliers, France) employing voltage pulsing mode, is performed at a residual pressure of 3×10^{-9} Pa and a specimen temperature of −223 °C, and with a pulse repetition frequency of 200 kHz, a pulse-voltage to dc-voltage ratio of 15%. The specimens for APT are prepared by using a standard two-stage electropolishing method at room temperature.[37] Data analysis is performed by using the Imago Visualization and Analysis Software (IVAS) software. Cu precipitates are identified using a 10 at.% Cu isoconcentration surface. For carbides, due to the small sizes and severe local magnification effect,[37] the pulse-evaporated matrix and precipitate atoms are overlapped, thus decreasing the measured C concentrations in carbides. So the carbide precipitates are identified using a 2 at.% C isoconcentration surface. The distributions of Cu precipitates and carbides are employed to visualize dislocations and subgrain boundaries, which are enclosed with selected

https://doi.org/10.1557/mrc.2012.21 Published online by Cambridge University Press

cylinders as regions of interest (ROIs) for further composition analysis. The two-dimensional (2D) concentration map and 1D composition profile are used to characterize the solute atoms variation along the dislocation line. The proxigram concentration profile is utilized to study the solute atoms distribution across the representative Cu precipitate/matrix heterophase interface.

Figure 1 gives a series of (HR)TEM images showing the microstructures of the quench-aged steel. The low-magnification bright-field TEM image in Fig. 1(a) reveals the lath-like morphology of martensitic structure, although some of the lath boundaries are hardly distinguished due to thermal aging. Figure 2(b) suggests that there is a high density of dislocations in the martensite lath interior. The defects of martensite lath boundaries and dislocations are considered to be from being tempered out during the brief thermal ageing for 4 h at 500 °C. The recovery of martensitic structure does not occur to the present ageing extent. The defects can induce the precipitation of Cu precipitates and carbides, which in turn impede the migration of dislocations to improve the strength.[38] HRTEM images in Figs. 1(c) and 1(d) reveal the fine dispersion of spherical precipitates on martensite lath boundary and dislocation, respectively. Energy dispersive x-ray spectroscopy demonstrates that the precipitates are Cu-rich and with an amount of Mn and Ni. The Cu precipitates are about 5 nm or below in size. The Moiré fringes around the Cu precipitates indicate the appearance of significant internal faulting, which is attributed to the elastic strains in association with the growth of Cu precipitates. Besides, the Cu precipitation on dislocation and at interface is consistent with the reduction of strain energy.

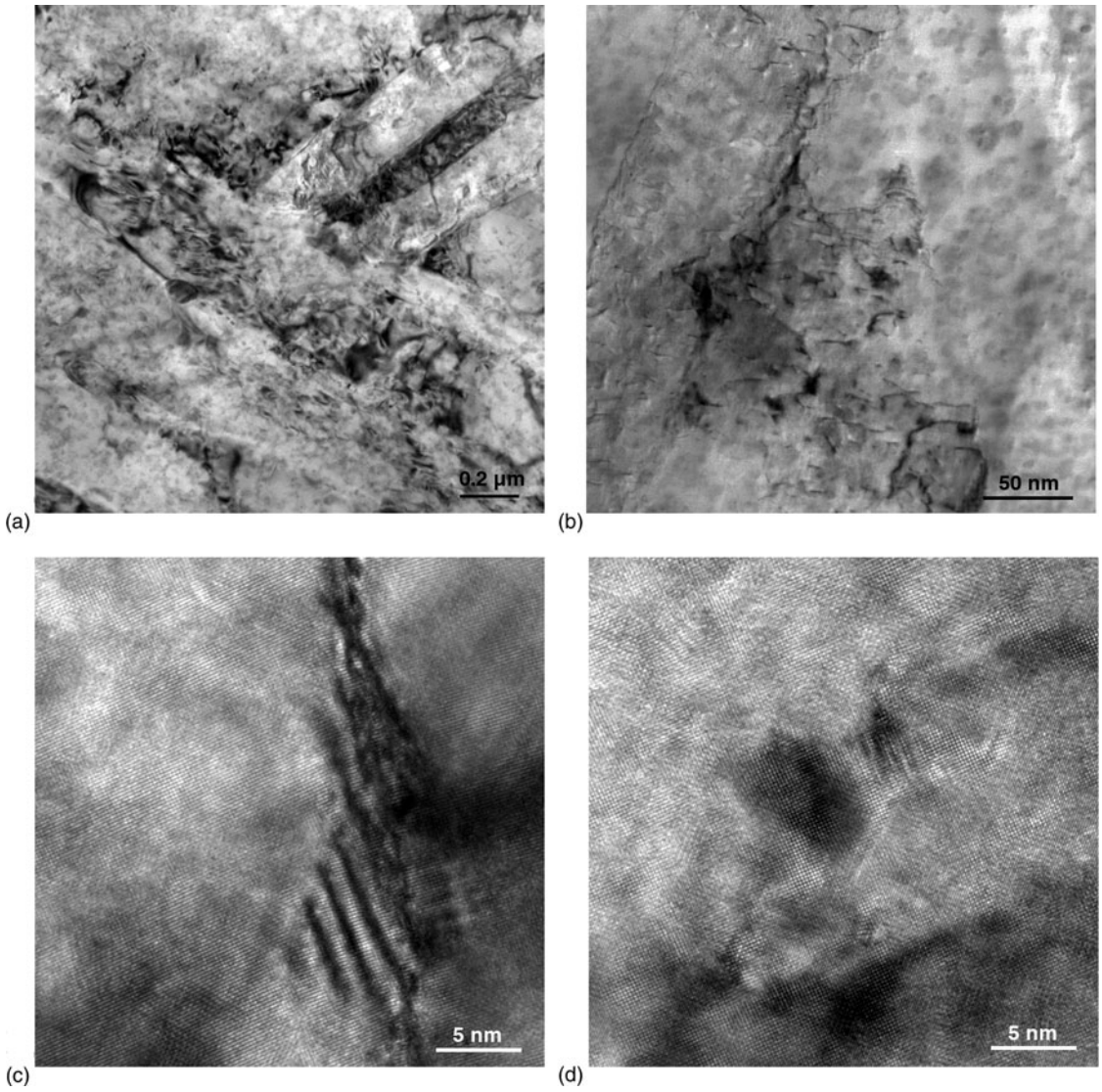


Figure 1. (HR)TEM images of Cu precipitates in dislocated martensitic microstructures isothermally aged at 500 °C for 4 h. (a) Lath-like structure. (b) Dislocation. (c) Cu precipitation at martensite lath boundary. (d) Cu precipitation on dislocation.

https://doi.org/10.1557/mrc.2012.21 Published online by Cambridge University Press

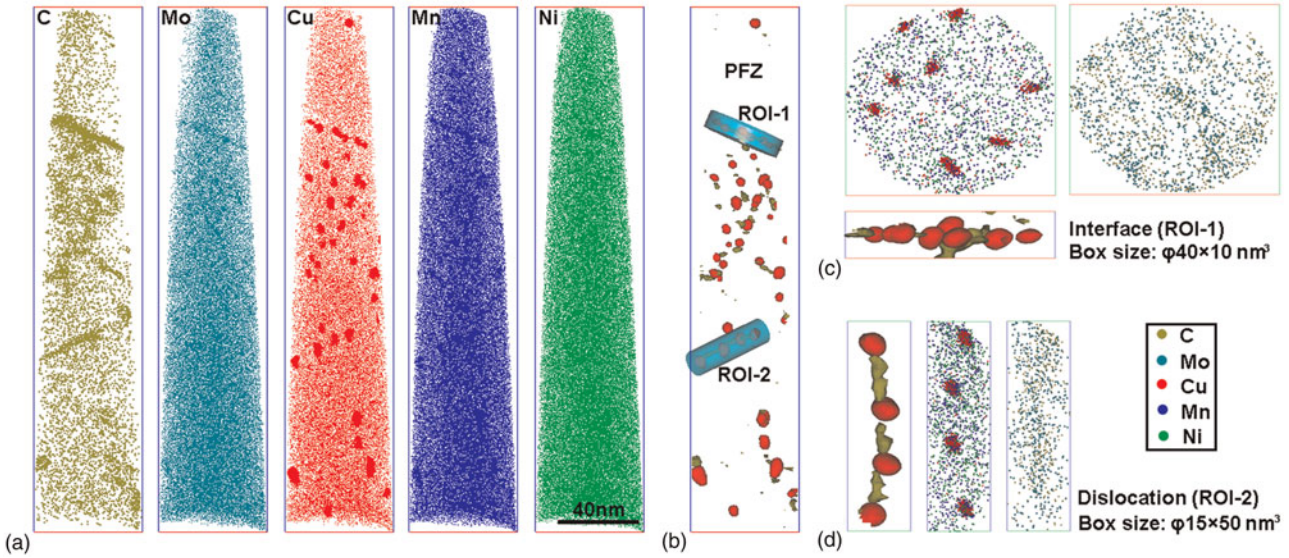


Figure 2. APT reconstructed 3D atom distribution maps of the HSLA steel isothermally aged at 500 °C for 4 h. (a) Spatial distribution of C, Mo, Cu, Mn and Ni atoms. (b) Cu precipitates and carbon-rich zones delineated by 10 at.% Cu and 2 at.% C isoconcentration surfaces (with a voxel size of 1.0 nm and a delocalization distance of 2.0 nm), respectively. Two subset boxes as ROIs (ROI-1 as interface and ROI-2 as dislocation) are selected for detailed analysis. A PFZ is detected near the interface. (c), (d) Side-view maps of interface and dislocation in (b) and the corresponding solute distribution in them.

APT results of the experimental steel aged at 500 °C for 4 h are displayed in Fig. 2. The 3D atom maps in Fig. 2(a) clearly show that the solute atoms are heterogeneously distributed, especially for C and Cu. In the C map, the C-rich planar feature corresponds to the martensite lath boundary that is also enriched with Mo, Cu, Mn and Ni. There are also many small regions with less concentrated enrichment, which are considered to be in association with Cottrell atmospheres of C or carbide clusters containing a small amount of Mo (see Mo atom map) at individual dislocations. The formation of these features usually occurs at the early stage of tempering[39,40] or even in an auto-tempering condition.[41] In the Cu map, the Cu-rich precipitates are distinctly observed and are seemingly located at the C-rich dislocations and lath boundary. The enrichment of Mn in Cu precipitates is also clearly observed. The Cu precipitation on C-rich dislocations and lath boundary is further depicted by the 10 at.% Cu and 2 at.% C isoconcentration surface map in Fig. 2(b). The Cu precipitates, with a number density of 1×10^{-23} m^{-3} and an average radius of 2.32 ± 0.97 nm, are formed either at the 2D defect of lath boundary or on the 1D defect of dislocation lines (see Supplementary material). However, the Cu precipitates are not homogeneously distributed in the whole analysis volume. In the upper subgrain interior, a precipitate-free zone (PFZ) is observed next to the lath boundary, and no C-enriched dislocation is detected in this region. Most of the Cu atoms diffuse from the upper subgrain interior to the subgrain boundary during thermal aging, leading to the formation of the Cu-depleted areas and the PFZ consequently. The lath boundary supplies a fast diffusion path for Cu and C to induce the nucleation of the Cu precipitates and carbides. So the configuration of defects is decisive for the precipitation morphology. At the same time, the Cu precipitation and C segregation reduce the energy of the subgrain interfaces and the dislocations, and thus reduce the driving force for the recovery and recrystallization of martensitic structure. The stabilization of defects by solute segregation has been reported.[42–44]

The average chemical compositions of Cu precipitates, matrix and PFZ are summarized in Table I. The Cu precipitates contain a large amount of Fe as high as to about 62 at.% and are rich in Ni and Mn, which is consistent with the previous studies.[30] Because of the co-precipitation of Cu precipitates and carbides at structural defects, additional C are usually included in the Cu precipitate when computing the Cu isoconcentration surfaces by IVAS, leading to higher C content in Cu precipitates. The left matrix contains naturally less Cu but a considerable amount of Ni and Mn. There is no obvious difference in the composition of the matrix and PFZ (just slightly lower in Cu, Ni, Mn and Mo). It seems that the martensite lath boundary next to the PFZ consumes more solute atoms to precipitate out than matrix dislocations do. Two ROIs cutting through the lath boundary [Fig. 2(c)] and dislocation [Fig. 2(d)] are selected for the analysis of the composition distribution around the structural defects. The enlarged isoconcentration surface maps further indicate the coprecipitation of Cu precipitates and carbides at the defects. However, the rotated atom maps of C (yellow), Mo (cyan), Cu (red), Mn (blue) and Ni (green) suggest that the Cu precipitate phases and Mo-containing carbide clusters are not intersoluble, i.e., these two features exist independently at the atomic level.

https://doi.org/10.1557/mrc.2012.21 Published online by Cambridge University Press

Table 1. The chemical compositions measured by APT in at.% of Cu precipitates, matrix and PFZ in Fig. 2.

	ε-Cu	Matrix	PFZ
C	0.116 ± 0.009	0.031 ± 0.001	0.029 ± 0.002
Cu	30.368 ± 0.091	0.216 ± 0.002	0.204 ± 0.005
Ni	3.289 ± 0.033	1.754 ± 0.003	1.737 ± 0.009
Mn	2.417 ± 0.030	0.746 ± 0.002	0.715 ± 0.002
Mo	0.405 ± 0.056	0.341 ± 0.003	0.283 ± 0.007
Cr	0.379 ± 0.022	0.555 ± 0.004	0.592 ± 0.010
Si	0.408 ± 0.014	0.500 ± 0.002	0.557 ± 0.005
Al	0.150 ± 0.008	0.030 ± 0.001	0.031 ± 0.002
P	0.022 ± 0.007	0.014 ± 0.001	0.015 ± 0.002
Fe	62.038 ± 0.095	95.355 ± 0.007	95.528 ± 0.010

Figure 3 gives the contour maps of C, Mo, Cu, Mn and Ni in ROI-2 [see Fig. 2(d)], showing the composition gradients in the vicinity of the selected dislocation. It is obviously seen that the C-decorated dislocation intersects with four Cu precipitates. The overlap of C and Mo suggests the formation of C–Mo clusters, which represent the early nucleation stage of carbides because of their low concentrations. Mn and Ni are prone to segregate to the Cu precipitates. But the distribution extents of the Mn and Ni are larger than that of copper, and a slight tail of these solute atoms into the matrix is also evident. Figure 4(a) is the corresponding 1D concentration profile along the length of dislocation line. The enrichments of Ni and Mn as well as depletion of C and Mo at the core of Cu precipitates are evident, which further indicates that the formation of carbides and Cu precipitates during thermal aging occurs independently. Figure 4(b) is the proxigram concentration profile showing solute distribution from the center of a selected Cu precipitates to the surrounding matrix. The figure reveals a diffuse Cu precipitate/matrix heterophase interface rather than the abrupt interface that is observed normally. And the Ni and Mn

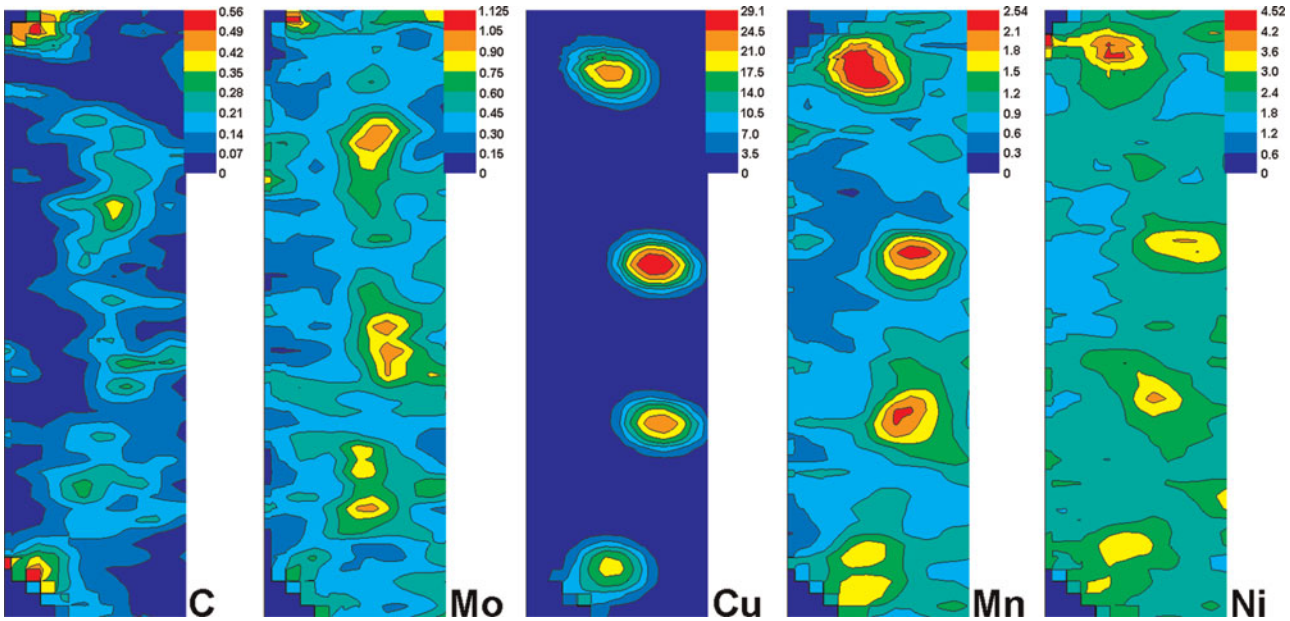


Figure 3. 2D concentration maps of C, Mo, Cu, Mn and Ni at the dislocation in ROI-1 in Fig. 2. C segregation to the dislocations and preferential precipitation of nanometer-sized Cu precipitates on the dislocation are evident.

https://doi.org/10.1557/mrc.2012.21 Published online by Cambridge University Press

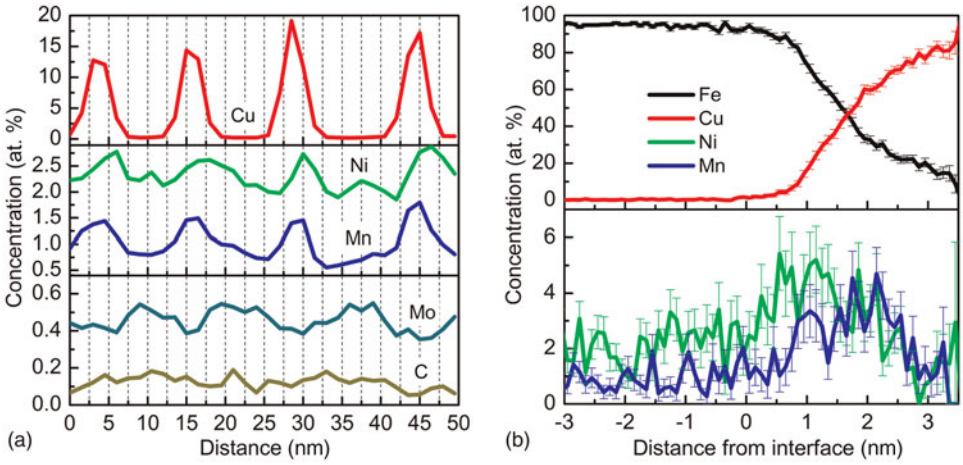


Figure 4. (a) 1D composition profile (at.%) of ROI-2 in Fig. 2 shows a composition variety along the dislocation line. (b) Proxigram concentration profiles (at.%) for Fe, Cu, Ni and Mn with respect to 10 at.% Cu isoconcentration surface of precipitates in ROI-2 in Fig. 2, showing the partitioning behaviors of Ni, Mn, Al and Si at the Cu precipitate/ferrite matrix heterophase boundary.

actually segregate at the precipitate/matrix heterophase interface.

In conclusion, Cu precipitation on dislocations and martensite laths interfaces has been directly observed by HRTEM and APT in quench-aged Cu-bearing HSLA steel. The C segregation and Cu precipitation occur simultaneously at the dislocations and interfaces, but the two features are not intersoluble and are independent in 3D distribution. The co-clustering of Mo with C indicates the early nucleation stage of carbides. The Cu precipitates are rich in Fe. Ni and Mn are prone to segregation at the Cu precipitate/matrix heterophase interface.

Acknowledgments

The authors are grateful for financial support of National Natural Science Foundation of China (Grant No. 50931003).

Supplementary materials

For supplementary material for this article, please visit http://dx.doi.org/10.1557/mrc.2012.21

References

1. S. Vaynman, D. Isheim, R. Prakash Kolli, S.P. Bhat, D.N. Seidman, and M.E. Fine: High-strength low-carbon ferritic steel containing Cu-Fe-Ni-Al-Mn precipitates. *Metall. Mater. Trans. A* **39**, 363 (2008).
2. Z. Zhang, C. Liu, Y. Wen, A. Hirata, S. Guo, G. Chen, M. Chen, and B. Chin: Influence of aging and thermomechanical treatments on the mechanical properties of a nanocluster-strengthened ferritic steel. *Metall. Mater. Trans. A* **43**, 351 (2012).
3. R.D.K. Misra, Z. Jia, R. O'Malley, and S.J. Jansto: Precipitation behavior during thin slab thermomechanical processing and isothermal aging of copper-bearing niobium-microalloyed high strength structural steels: the effect on mechanical properties. *Mater. Sci. Eng. A* **528**, 8772 (2011).
4. A. Ghosh, B. Mishra, S. Das, and S. Chatterjee: An ultra low carbon Cu bearing steel: influence of thermomechanical processing and aging heat treatment on structure and properties. *Mater. Sci. Eng. A* **374**, 43 (2004).
5. A. Ghosh, B. Mishra, S. Das, and S. Chatterjee: Microstructure, properties, and age hardening behavior of a thermomechanically processed ultralow-carbon Cu-bearing high-strength steel. *Metall. Mater. Trans. A* **36**, 703 (2005).
6. A. Saha, J. Jung, and G. Olson: Prototype evaluation of transformation toughened blast resistant naval hull steels: Part II. *J. Computer-Aided Mater. Des.* **14**, 201 (2007).
7. S. Thompson and G. Krauss: Copper precipitation during continuous cooling and isothermal aging of a710-type steels. *Metall. Mater. Trans. A* **27**, 1573 (1996).
8. Q.D. Liu, W.Q. Liu, and X.Y. Xiong: Correlation of Cu precipitation with austenite–ferrite transformation in a continuously cooled multicomponent steel: an atom probe tomography study. *J. Mater. Res.* **27**, 1060 (2012).
9. Q.D. Liu and S.J. Zhao: Comparative study on austenite decomposition and Cu precipitation during continuous cooling transformation. *Metall. Mater. Trans. A* (in press). DOI: 10.1007/s11661-012-1383-2.
10. M. Mujahid, A.K. Lis, C.I. Garcia, and A.J. DeArdo: HSLA-100 steels: Influence of aging heat treatment on microstructure and properties. *J. Mater. Eng. Perform.* **7**, 247 (1998).
11. A. Deschamps, M. Militzer, and W.J. Poole: Comparison of precipitation kinetics and strengthening in an Fe-0.8% Cu alloy and a 0.8% Cu-containing low-carbon steel. *ISIJ Int.* **43**, 1826 (2003).
12. A. Deschamps, M. Militzer, and W.J. Poole: Precipitation kinetics and strengthening of a Fe-0.8 wt% Cu alloy. *ISIJ Int.* **41**, 196 (2001).
13. J. Takahashi, K. Kawakami, and Y. Kobayashi: Consideration of particle-strengthening mechanism of copper-precipitation-strengthened steels by atom probe tomography analysis. *Mater. Sci. Eng. A* **535**, 144 (2012).
14. G.R. Speich and W.C. Leslie: Tempering of steel. *Metall. Trans.* **3**, 1043 (1972).
15. H.A.H. Duparc, R.C. Doole, M.L. Jenkins, and A. Barbu: A high-resolution electron microscopy study of copper precipitation in Fe-1.5 wt% Cu under electron irradiation. *Philos. Mag. Lett.* **71**, 325 (1995).
16. Y. Le Bouar: Atomistic study of the coherency loss during the b.c.c.-9R transformation of small copper precipitates in ferritic steels. *Acta Mater.* **49**, 2661 (2001).
17. T.H. Lee, Y.O. Kim, and S.J. Kim: Crystallographic model for bcc-to-9R martensitic transformation of Cu precipitates in ferritic steel. *Philos. Mag.* **87**, 209 (2007).
18. W. Wang, B.X. Zhou, G. Xu, D.F. Chu, and J.C. Peng: High-resolution electron microscopy characterization of 2H and 9R variant in the ferritic steels containing copper. *Mater. Charact.* **62**, 438 (2011).

https://doi.org/10.1557/mrc.2012.21 Published online by Cambridge University Press

19. R. Monzen, M. Iguchi, and M.L. Jenkins: Structural changes of 9R copper precipitates in an aged Fe-Cu alloy. *Philos. Mag. Lett.* **80**, 137 (2000).
20. R. Monzen, M.L. Jenkins, and A.P. Sutton: The bcc-to-9R martensitic transformation of Cn precipitates and the relaxation process of elastic strains in an Fe-Cu alloy. *Philos. Mag. A* **80**, 711 (2000).
21. P.J. Othen, M.L. Jenkins, G.D.W. Smith, and W.J. Phythian: Transmission electron microscope investigations of the structure of copper precipitates in thermally-aged Fe-Cu and Fe-Cu-Ni. *Philos. Mag. Lett.* **64**, 383 (1991).
22. J.J. Blackstock and G.J. Ackland: Phase transitions of copper precipitates in Fe-Cu alloys. *Philos. Mag. A* **81**, 2127 (2001).
23. D. Isheim, R.P. Kolli, M.E. Fine, and D.N. Seidman: An atom-probe tomographic study of the temporal evolution of the nanostructure of Fe-Cu based high-strength low-carbon steels. *Scripta Mater.* **55**, 35 (2006).
24. S.R. Goodman, S.S. Brenner, and J.R. Low: An FIM-atom probe study of the precipitation of copper from Iron-1.4 at. pct copper. Part II: atom probe analyses. *Metall. Mater. Trans. B* **4**, 2371 (1973).
25. M. Schober, E. Eidenberger, P. Staron, and H. Leitner: Critical consideration of precipitate analysis of Fe-1 at.% Cu using atom probe and small-angle neutron scattering. *Micros. Microanal.* **17**, 26 (2011).
26. D. Isheim, M.S. Gagliano, M.E. Fine, and D.N. Seidman: Interfacial segregation at Cu-rich precipitates in a high-strength low-carbon steel studied on a sub-nanometer scale. *Acta Mater.* **54**, 841 (2006).
27. M.D. Mulholland and D.N. Seidman: Multiple dispersed phases in a high-strength low-carbon steel: an atom-probe tomographic and synchrotron x-ray diffraction study. *Scripta Mater.* **60**, 992 (2009).
28. H. Nakamichi, K. Yamada, K. Sato: Sub-nanometre elemental analysis of Cu cluster in Fe–Cu–Ni alloy using aberration corrected STEM-EDS. *J. Micros.* **242**, 55 (2011).
29. R.P. Kolli and D.N. Seidman: The temporal evolution of the decomposition of a concentrated multicomponent Fe-Cu-based steel. *Acta Mater.* **56**, 2073 (2008).
30. M. Schober, E. Eidenberger, H. Leitner, P. Staron, D. Reith, and R. Podloucky: A critical consideration of magnetism and composition of (bcc) Cu precipitates in (bcc) Fe. *Appl. Phys. A* **99**, 697 (2010).
31. A.B. Edwards, K.J. Roberts, S. Pizzini, and W.J. Phythian: The local atomic environment of Cu and Ni in Fe-Cu-Ni alloys following thermal ageing and neutron irradiation: a study using fluorescence mode x-ray absorption fine-structure spectroscopy. *Philos. Mag. A* **79**, 1295 (1999).
32. M.K. Miller: APT characterization of solute segregation to individual dislocations. *TMS Lett.* **1**, 19 (2004).
33. M.K. Miller: Atom probe tomography characterization of solute segregation to dislocations. *Micros. Res. Tech.* **69**, 359 (2006).
34. M. Miller: Atom probe tomography characterization of solute segregation to dislocations and interfaces. *J. Mater. Sci.* **41**, 7808 (2006).
35. M.K. Miller: Interface analysis with the three-dimensional atom probe. *Surf. Interface Anal.* **31**, 593 (2001).
36. D. Blavette, E. Cadel, A. Fraczkiewicz, and A. Menand: Three-dimensional atomic-scale imaging of impurity segregation to line defects. *Science* **286**, 2317 (1999).
37. M.K. Miller: *Atom Probe Tomography: Analysis at the Atomic Level* (Kluwer Publishing/Plenum Press, New York, NY, 2000).
38. A.J. Ardell: Precipitation hardening. *Metall. Mater. Trans. A* **16**, 2131 (1985).
39. Q.D. Liu, W.Q. Liu, Z.M. Wang, and B.X. Zhou: 3D atom probe characterization of alloy carbides in tempering martenite I. Nucleation. *Acta Metall. Sin.* **45**, 1281 (2009).
40. Q.D. Liu, W.Q. Liu, and S.J. Zhao: Solute behavior in the initial nucleation of V- and Nb-containing carbide. *Metall. Mater. Trans. A* **42**, 3952 (2011).
41. B. Hutchinson, J. Hagstrom, O. Karlsson, D. Lindell, M. Tornberg, F. Lindberg, and M. Thuvander: Microstructures and hardness of as-quenched martensites (0.1–0.5%C). *Acta Mater.* **59**, 5845 (2011).
42. R. Kirchheim: Grain coarsening inhibited by solute segregation. *Acta Mater.* **50**, 413 (2002).
43. R. Kirchheim: Reducing grain boundary, dislocation line and vacancy formation energies by solute segregation: II. Experimental evidence and consequences. *Acta Mater.* **55**, 5139 (2007).
44. R. Kirchheim: Reducing grain boundary, dislocation line and vacancy formation energies by solute segregation. I. Theoretical background. *Acta Mater.* **55**, 5129 (2007).

https://doi.org/10.1557/mrc.2012.21 Published online by Cambridge University Press